OPTICS

Topological beaming of light

Ki Young Lee[1], Seungjin Yoon[2], Seok Ho Song[1], Jae Woong Yoon[1]*

Nanophotonic light emitters are key components in numerous application areas because of their compactness and versatility. Here, we propose a topological beam emitter structure that takes advantage of submicrometer footprint size, small divergence angle, high efficiency, and adaptable beam shaping capability. The proposed structure consists of a topological junction of two guided-mode resonance gratings inducing a leaky Jackiw-Rebbi state resonance. The leaky Jackiw-Rebbi state leads to in-plane optical confinement with funnel-like energy flow and enhanced emission probability, resulting in highly efficient optical beam emission. In addition, the structure allows adaptable beam shaping for any desired positive definite profiles by means of Dirac mass distribution control, which can be directly encoded in lattice geometry parameters. Therefore, the proposed approach provides highly desirable properties for efficient micro–light emitters and detectors in various applications including display, solid-state light detection and ranging, laser machining, label-free sensors, optical interconnects, and telecommunications.

INTRODUCTION

Topological interface states (*1*–*4*) reveal unique physical properties with remarkably high robustness against local parametric or environmental disturbances (*5*, *6*). The mathematical analogy of the electronic equation of motions in solids to the optical wave equation in photonic nanostructures has triggered extensive investigations on photonic topological phenomena. Photonic topological systems (*7*–*13*) provide greatly enhanced experimental feasibility in configuring desired potential distributions for fundamental study and a wide variety of promising applications to telecommunications, data processing, sensors, and many others.

Of our particular interest within this context are the non-Hermitian topological states in leaky photonic systems (*14*–*17*). In leaky photonic systems such as guided-mode resonance (GMR) gratings, thin-film photonic crystals, and metasurfaces, the non-Hermiticity naturally arises because of the inherent radiative decay processes toward the radiation continuum. These decay channels in the optical far field can be efficiently used to coherently control or probe certain desired topological states for their spectral intensity, phase, and polarization properties, which are key constituent elements in nanophotonic device engineering. Such possibilities have been recently demonstrated in part with polarization-vortex beam generation (*18*), optical wavefront control (*19*), and out-of-plane Jackiw-Rebbi (JR) state resonances (*17*, *20*). Considering the great technological potential of topological device engineering in photonics, further associated studies are highly desirable to create novel free-space optical elements that take advantage of the unique topological properties hardly obtainable from conventional approaches.

In pursuit of novel far-field optical properties associated with non-Hermitian topological photonic phenomena here, we show that a topological junction metasurface of two GMR gratings acts as an efficient submicrometer light emitter having highly desirable characteristics of small angular divergence, high quantum efficiency, and adaptable beam shaping capability. Previous attempts to create a well-directed source of light mostly rely on the excitation of surface waves from a single aperture surrounded by a periodic corrugation such as bull's eye metallic films (*21*, *22*) and photonic crystal waveguides with an appropriate edge termination (*23*–*25*). In contrast, we use a junction consisting of two topologically distinct GMR gratings directly adjacent to each other in the absence of any aperture. In such a structure, a leaky JR state at the junction emits a narrow beam of light from internal isotropic sources driven by the cavity–quantum electrodynamics (QED) coupling and electromagnetic funneling effects. For an appropriately optimized design, the combined driving mechanisms lead to beam divergence approaching the fundamental minimum due to the position-momentum uncertainty relation and enhanced emission rate by a factor of 10. In addition, the structure allows beam shaping for an arbitrarily desired positive definite profile by means of grating fill factor controls. We provide a fundamental theory of the topological beam emission and rigorous numerical analyses of experimentally presumable structures operating in the visible domain.

RESULTS

Leakage radiation from a JR state

We consider a leaky JR state localized at a photonic topological junction metasurface as schematically illustrated in Fig. 1A. The structure has a high-index (n_c) film with total thickness $d = d_1 + d_2$ and a low-index (n_d) surrounding medium. We take different values for period a_L or a_R and width W_L or W_R of the grating ridges on the left (L) or right (R) side of the junction such that the left and right regions are in different topological phases at the second-order Bragg reflection condition. In such condition, the first-order diffraction from the JR state leads to a beam of leakage radiation toward the surrounding background media (*20*). Characteristic features of this leakage radiation are the subject of our major interest here.

As an exemplary trial case, we take parameters d_1 = 60 nm, d_2 = 40 nm, n_c = 2.6 (TiO_2), n_d = 1.45 (SiO_2), W_L = 95 nm, a_L = 360 nm, W_R = 227 nm, and a_R = 325 nm. This parameter set is chosen for a leaky JR state resonance under transverse-electric (TE)-polarized light incidence at a wavelength of 633 nm as shown in Fig. 1B.

[1]Department of Physics, Hanyang University, Seoul, 133-791, Republic of Korea. [2]James Watt School of Engineering, University of Glasgow, Glasgow G12 8QQ, UK. *Corresponding author. Email: yoonjw@hanyang.ac.kr

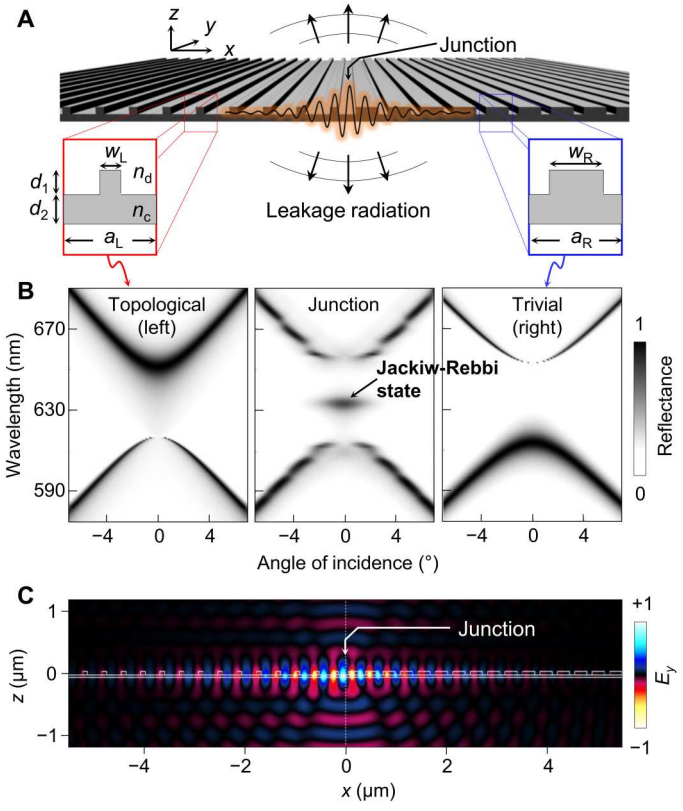

Fig. 1. Fundamental properties of the leaky JR state in a topological junction metasurface. (**A**) Schematic of a topological junction consisting of two different thin-film subwavelength gratings. (**B**) Angle-dependent reflection spectra for the left unit cell in the topological phase (left), the right unit cell in the trivial phase (right), and their junction (middle). (**C**) Electric field amplitude E_y of the leaky JR state at wavelength λ_{JR} = 633 nm. We use the finite element method (Comsol Multiphysics) for this calculation.

We provide the angle-dependent reflection spectra for the left lattice in the topological phase and right lattice in the trivial phase. The two spectra show characteristic band-edge state flip between the non–leaky bound states in the continuum (BIC) (vanishing bandwidth) and leaky GMR (doubled bandwidth) as a signature of the topological phase transition due to a π-phase jump in the second-order Bragg reflection at a certain critical value (*20*) in fill factor $F = W/a$.

In analogy to the zero-energy state solution of the Dirac equation, a junction of these two lattices supports a leaky JR state at the center of the bandgap as indicated in the angle-dependent spectrum in the middle of Fig. 1B. We use a supercell including 50 lattice periods in this calculation. See Materials and Methods and section S2-1 for details of the numerical calculation method and description of the JR state resonance peak depending on the incident light configurations. In Fig. 1C, we show the electric field distribution of the leaky JR state as a solution of an eigenvalue problem using the finite element method (FEM) simulation. It reveals the in-plane localization at the junction and leakage radiation toward the surrounding medium.

Optical near-field and emission patterns of this leaky JR state can be conveniently described by the diffractive coupled-mode theory in analogy to the one-dimensional Dirac equation (*20*). The theory describes the transversal electric field (E_y) for the JR state as a localized standing wave

$$\psi_{JR} = u(z)\,(e^{iqx} + ie^{-iqx})f(x) \tag{1}$$

where $u(z)$ is the cross-sectional wave function of the guided mode, $q = 2\pi/a$ is the grating vector, and $f(x) = \exp.[\int^x - m(x')dx']$ is a localization envelope function with Dirac mass parameter

$$m(x) \approx n_g \pi \lambda_0^{-1}[G(x) + iQ(x)^{-1}] \tag{2}$$

Here, n_g is the group index of the guided mode, λ_0 is the bandgap center wavelength, $Q \approx \pi c(\lambda_0\gamma)^{-1}$ is the GMR Q factor with γ being the radiation decay rate, and $G = (\lambda_a - \lambda_s)\lambda_0^{-1}$ is the relative bandgap width with λ_a and λ_s denoting band-edge wavelengths for the antisymmetric (BIC) and symmetric (leaky GMR) standing guided modes with respect to the mirror symmetry plane of the grating, respectively. m is a key parameter that determines the topological phase of the structure such that $Re(m) \propto G > 0$ for the trivial phase while $Re(m) \propto G < 0$ for the topological phase. Therefore, the spectral flip of the leaky GMR and BIC at the two band edges λ_s and λ_a indicates the onset of the topological phase transition as we see in Fig. 1B. Considering a junction of two topologically distinguished GMR gratings with identical bandgap size and location, we assume $m(x < 0) = m_L$, $m(x > 0) = m_R$, and $m_R = -m_L = m_{JR} = \pi n_g \lambda_0^{-1}(G_0 + iQ_0^{-1})$ for the sake of simplicity hereafter.

Once ψ_{JR} is excited, it emits zero-order wave ψ_0 through the −1-order diffraction from the e^{iqx} component and the +1-order diffraction from the ie^{-iqx} component in Eq. 1. A superposition of these two contributions leads to an expression for ψ_0 as

$$\psi_0 = -(1+i)\varepsilon_1 k_0^2 \int G(z,z')u(z')dz'\, f(x) \tag{3}$$

where $k_0 = 2\pi\lambda_0^{-1}$, ε_1 is the first harmonic spatial Fourier transform of $\varepsilon(x)$, $G(z,z')$ is a one-dimensional Green function for a planar source parallel to the xy plane, and the integration is running over the grating layer. Consequently, the leakage radiation ψ_{rad} in the optical far field is described by the diffraction theory as

$$\psi_{rad} = \frac{n_d}{\lambda_0}\int_{-\pi/2}^{+\pi/2} F(\theta)e^{in_d k_0(x\sin\theta + z\cos\theta)}\cos\theta\, d\theta \tag{4}$$

$$F_f(\theta) = \frac{1}{\sqrt{2\pi}}\int_{-\infty}^{+\infty} f(x)\, e^{-in_d k_0 x\sin\theta}dx \tag{5}$$

See section S1 for details of the mathematical treatment for Eqs. 3 to 5. Angular distribution $F_f(\theta)$ of the leakage radiation in the optical far field is simply a spatial Fourier transform of the normalized bidirectional decaying exponential function $f(x) = \sqrt{m_{JR}}$ exp.$(-m_{JR}|x|)$ and is thereby given by Lorentzian distribution

$$F_f(\theta) = \frac{(\sigma/2)^2}{\sin^2\theta + (\sigma/2)^2}F_f(0) \tag{6}$$

with angular beam width parameter $\sigma \approx (n_g n_d^{-1})|G_0|$ in the narrow resonance limit of $|G_0| >> Q_0^{-1}$. For the simulated case in Fig. 1B, we estimate the relative bandgap width $G_0 \approx 6.3 \times 10^{-2}$, and this yields the angular beam width $\sigma \approx 7.3°$ in free space. Therefore, a

leaky JR state at the second-order Bragg condition potentially creates a narrow-angle beam emission for waveguide gratings with moderate design parameters.

Associated with the narrow beam emission from the leaky JR state, we investigate the emission properties of light sources in the vicinity of the topological junction. We calculate the radiation pattern $|E_y(x,z)|^2$ from a coherent light source array at the JR state resonance condition ($\lambda = \lambda_0 = 633$ nm) for the topological junction in Fig. 1C. In this calculation, we use the FEM and assume a periodic array of isotropic cylindrical light sources over a 10-μm-wide plane of maximal guided-mode intensity in the middle of the waveguide layer. See Materials and Methods and section S2-2 for details of the simulation method. The calculated radiation pattern in Fig. 2A shows a narrow beam emitted in the optical far field. Note in Fig. 2A that the far-field emission pattern is symmetric with respect to the *yz* plane although the structure is basically an asymmetric junction of two different waveguide gratings. This property is attributed to the symmetry of the JR state envelope and identical radiation strengths in the two grating regions as magnitudes of the Dirac mass parameters in their real and imaginary parts are almost identical in the two grating regions about the junction. A slight asymmetry in the radiation pattern is due to the small difference in γ (imaginary part of the Dirac mass parameter) for the two structures. If we appropriately design a structure so that the two grating regions have exactly identical Dirac mass parameters, the emitted beam should be ideally symmetric as shown in fig. S3.

The narrow beam emission from isotropic light sources exactly follows the diffraction properties of the leakage radiation from the JR state. According to Eqs. 1 and 4, the lateral profile $f(x)$ of the JR state and its angular spectrum $F_f(\theta)$ are the Fourier transform pair of each other. Therefore, their effective sizes Δx and $\Delta\theta$ in the root mean square sense follow an uncertainty-like relation

$$\Delta x \cdot \Delta k_x = n_d k_0 \cos\theta \, \Delta x \cdot \Delta\theta = 1/\sqrt{2} \tag{7}$$

This is close to the minimum transform-limited uncertainty product of 1/2, and a highly directional beam is thus emitted from a strongly localized radiation area of the JR state, as confirmed from our simulated cases with different bandgap width $g = |G_0|\lambda_0$ values in Fig. 2 (B to D). Details of calculation parameters of the numerical analysis are provided in Table 1. We note in Fig. 2 (B and C) that the bandgap width $g = 80$ nm yields $\Delta x = 670$ nm and $\Delta\theta = \sin^{-1}(\Delta k_x/k_0) = 6°$, implying a highly directional emission from a submicrometer surface region. Therefore, this property can be efficiently used for directional submicrometer display pixels, which are technically unavailable yet but highly desirable for many applications (*26*).

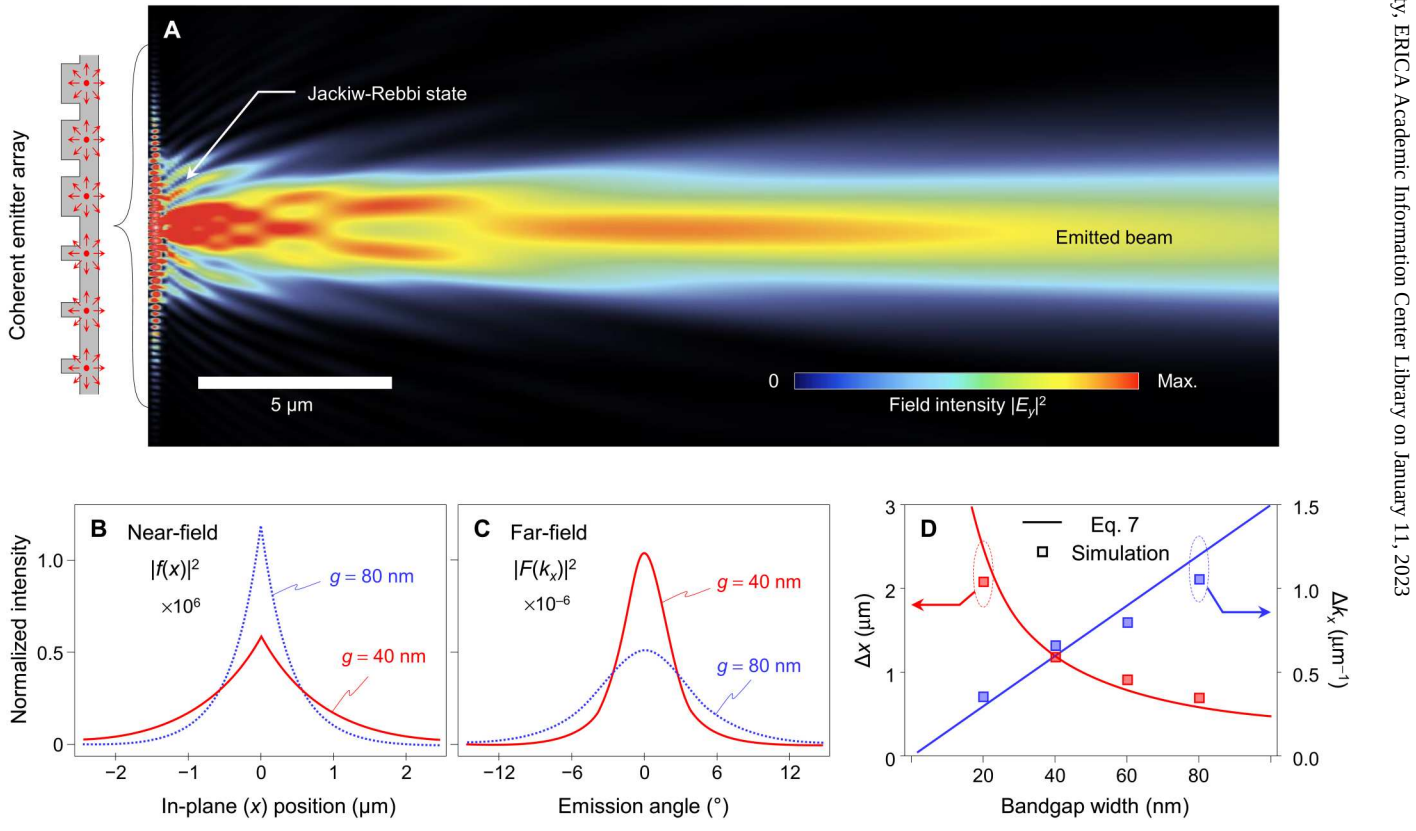

Fig. 2. Far-field properties of light from isotropic light sources near the topological junction metasurface. (**A**) Far-field radiation pattern $|E_y|^2$ from an array of isotropic emitters that are evenly placed inside the device region from $x = -5$ to 5 μm at $z = 0$. (**B** and **C**) Normalized localization envelope function $f(x)$ and its spatial Fourier transform $F(k_x)$ for the emission angle θ in free space, respectively. (**D**) Position–wave vector uncertainty relation of the leaky JR state according to bandgap size g.

Table 1. Details of structural parameters and their numerical results in Fig. 2D.

Bandgap width (g)	Ridge width ($W_{L,R}$)	Period ($a_{L,R}$)	Thickness ($d_{1,2}$)	Refractive index ($n_{c,d}$)	Δx	Δk_x
20 nm	130, 183 nm	350, 337 nm	60, 40 nm	2.6, 1.45	2.07 μm	0.34 μm^{-1}
40 nm	95, 227 nm	360, 325 nm	60, 40 nm	2.6, 1.45	1.08 μm	0.65 μm^{-1}
60 nm	104, 158 nm	400, 365 nm	100, 0 nm	3.0, 1.45	0.89 μm	0.79 μm^{-1}
80 nm	80, 167 nm	410, 360 nm	100, 0 nm	3.0, 1.45	0.67 μm	1.05 μm^{-1}

Funneling and Purcell effects

According to the emitter array analysis in Fig. 2, we confirm that the primary radiation channel of an emitter in the vicinity of the topological junction is not the isotropic mode but the JR state and its leakage radiation in a narrow angular range. This beaming effect involves two enhancement mechanisms. One is energy-flow funneling and the other is the cavity-QED effect, i.e., the Purcell enhancement.

The energy-flow funneling is understood from the characteristic form of the leaky JR state wave function. ψ_{JR} in Eq. 1 as a frequency-domain electric field wave function results in time-average in-plane Poynting vector component $\langle S_x \rangle_t = 2Re(E_y H_z^*)$ as

$$\langle S_x \rangle_t = -\mathrm{sgn}(x)\ 4m'' e^{-2m'|x|}[1 + \sin(2qx)]\ |\ u(z)\ |^2 \qquad (8)$$

where $m'' = \mathrm{Im}(m_{JR})$ and $m' = Re(m_{JR})$. In this expression, the leaky JR state exerts an in-plane energy flow directed towards the junction at $x = 0$ like a funnel, as confirmed in the calculated Poynting vector distribution in Fig. 3A. We note in Eq. 8 that the magnitude of this energy flow funneling is proportional to radiative decay rate $m'' = \pi n_g (\lambda_0 Q)^{-1}$ of the GMR. It implies that the nonuniform strength of the out-of-plane radiation produces an in-plane energy flow such that the local flow directs toward a stronger radiation point from the neighboring weaker radiation region.

The effect of the funnel-like energy flow is more prominent in the energy flow distribution from a single emitter. In Fig. 3 (B and C), we show two single-emitter cases with different emitter positions (x_P) from the junction. We see in both cases for $x_P = 1$ μm and 2 μm that most of the emitted energy inside the waveguide directs toward the junction and the out-of-plane radiation is generated in the form of leakage radiation of the JR state. This numerical observation provides a causal explanation for the beaming of a coherent array of emitters in Fig. 2, corresponding to a coherent superposition of the periodically distributed single-emitter cases.

In further consideration, the funnel-like energy flow is effective only for the emitters under the influence of the JR state, i.e., emitters within funneling boundaries (*27*–*29*). To see the effective funneling region, we calculate emission intensity distribution as a function of the emitter position x_P from the junction, as shown in Fig. 3D. We set an observation plane at 3.5 μm above the waveguide surface and calculate lateral intensity distribution on the observation plane as a function of emitter position x_P. See Materials and Methods and section S2-3 for details of the calculation method. We consider a funneling boundary as a maximal lateral displacement $|x_P|$ at which

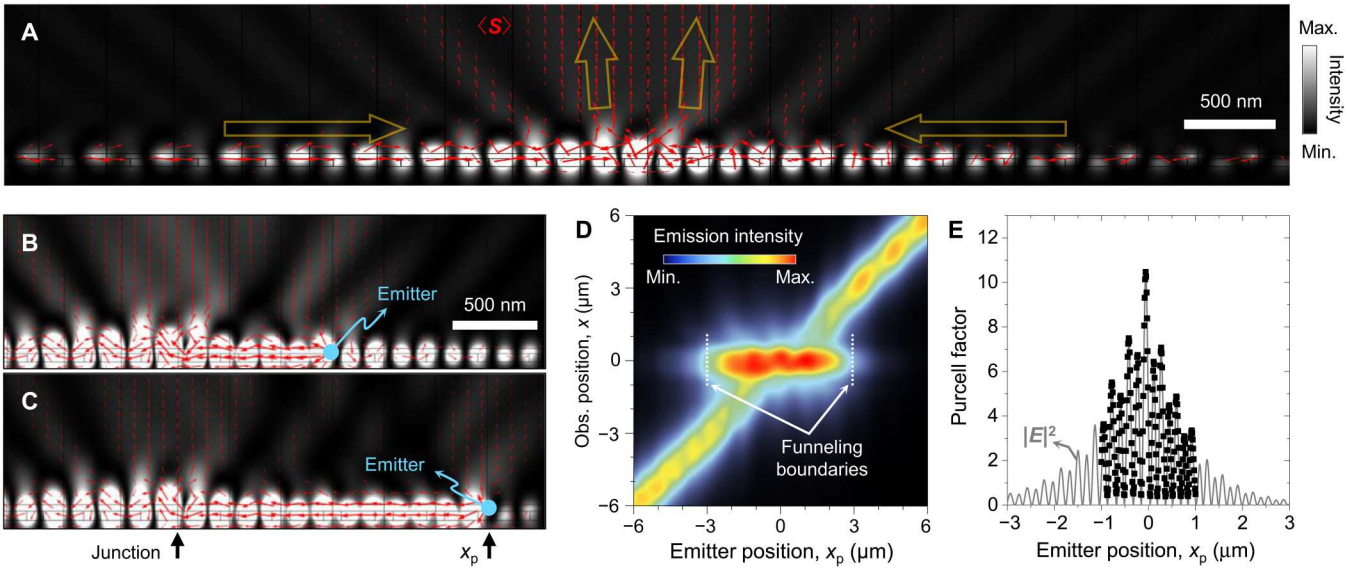

Fig. 3. Electromagnetic funneling and Purcell enhancement of internal sources. (**A**) Optical power-flow (time-average Poynting vector $\langle \boldsymbol{S} \rangle_t$; red arrows) distribution for a topological junction with bandgap size $g = 40$ nm in reference to the near-field intensity distribution (gray-level density). (**B** and **C**) Optical power flow excited by a single isotropic source 1 and 2 μm away from the junction ($x_P = 1$ and 2 μm), respectively. (**D**) Source-position (x_P)–dependent far-field intensity distribution on an observation plane 3.5 μm above the grating surface as a function of x_P. (**E**) Purcell factor distribution in comparison with the near-field intensity distribution associated with the JR state.

emission from the source effectively causes beaming at the junction interface. The funneling boundaries are clearly identified at $x_P \asymp \pm 3$ μm within which the maximum emission intensity position stays at $x = 0$ (the lateral position on the observation plane straight above the junction). The identified funneling boundary diameter is approximately $2m'^{-1}$, and this value corresponds to a domain accommodating around 98% of the field energy in the JR state such that $\int_{-xp}^{xp} |f(x)|^2 dx = 0.98$. The funneling boundary diameter represents a lateral range of sources that produces the desired beaming effect at a substantial magnitude. Therefore, it can be regarded as a minimally possible device footprint size for the efficient beaming effect. We note however that a submicrometer beam produced from the structure does not necessarily imply a submicrometer footprint size because the funneling boundary diameter is larger than beam width Δx. For example, the funneling boundary diameter for the submicrometer beam case Δx = 670 nm in Table 1 is estimated as 1.6 μm according to Eq. 2 for the Dirac mass parameter value.

The emission intensity distribution in Fig. 3D also suggests the Purcell enhancement at a remarkable magnitude because the peak emission intensity is significantly higher within the funneling boundaries. The red area within the funneling boundaries is the enhanced emission region. In Fig. 3E, we show the calculated Purcell factor distribution in comparison with the electric field intensity $|\mathbf{E}|^2$ profile associated with the JR state. We use the radiative power comparison method (*30*) in this calculation. The calculated Purcell factor follows the $|\mathbf{E}|^2$ profile as predicted by Fermi's golden rule, and its peak value at the junction goes beyond 10, implying that the emission toward the JR state within the mode field diameter is about five times stronger on average than that into the isotropic free-space radiation. Therefore, we conclude that the proposed topological beam emission is driven by the Purcell enhancement and funneling effect as characteristic properties of a leaky JR state.

We also present a comparison of the Purcell factors for the GMR and JR states in fig. S7. This comparison suggests that the JR state has a relatively larger Purcell factor than the GMR state under the same structural condition because of its smaller mode volume. For further improvement of the Purcell factor, we point out two requirements. One is the mode-volume reduction, which is readily obtainable by increasing the magnitude of the Dirac mass parameter for the lateral confinement and increasing the effective index of the guided mode for the vertical confinement. The other is enhancement in the radiation Q factor. The radiation Q factor can be substantially enhanced by reducing the leakage radiation rate with appropriate modification in the grating geometry so that the first-order diffraction amplitude takes a smaller value. Therefore, the Purcell factor for a JR state resonance can be remarkably boosted by taking certain appropriate design optimization processes for optimal Fourier harmonic amplitudes of the dielectric constant distribution, high effective index, and maximal bandgap width.

In a practical point of view, it is important to consider external sources for the proposed beaming effect. In principle, one should be able to produce a remarkable beaming effect from external sources if the sources are placed within the mode field region of the JR state where the funneling effect and Purcell enhancement are favorably significant. Even for relatively distant sources away from the waveguide core, one may include certain structural modifications so that the JR state stretches a significant portion of its mode field toward the source. Such modifications include reducing the index contrast between the core and source-side clad, reducing effective index of the guided mode, introducing vertically coupled multilayer waveguide structures, and many others.

Adaptable beam shaping

Beam shaping is an important issue for many applications because light sources have their own characteristic beam profiles independent of the required specifications for desired uses in general. In this respect, the proposed topological beaming effect provides some possibility of beam shape control directly from the source. Although we have treated a specific m distribution, which is a piecewise constant with a step at the junction, and the subsequent localization profile follows a simple bidirectional exponential function, an arbitrary $m(x)$ distribution can be chosen for a certain desired localization profile $f(x)$ as far as m changes its sign in the region of localization. For a given desired localization profile $f(x)$, the basic theory of a JR state yields the corresponding Dirac mass distribution

$$m(x) = -\frac{1}{f}\frac{df}{dx} \tag{9}$$

with constraints $m(0) = 0$ and $f(x) > 0$. Because $f(x)$ itself is the beam profile of leakage radiation from a JR state in our proposed case of the second stop-band condition, any positive definite beam profile, in principle, can be created by appropriately distributing $m(x)$ due to Eq. 9.

Equation 9 describes the Dirac mass distribution required for generating the desired beam profile f. A required Dirac mass distribution can be mapped onto a corresponding fill factor distribution. Basically, the Dirac mass in our case is the difference between rates of the intermodal coupling through the two sequential first-order diffraction processes and the single second-order diffraction process (*20*), implying that it is adjustable with certain structure geometry parameters associated with relative strengths of the first- and second-order diffraction amplitudes, i.e., grating bar fill factor F in our case. In particular, the Dirac mass parameter can be expressed in terms of F as

$$m(x) = \frac{\pi n_g}{\lambda_0}\Delta\varepsilon F[C_1\Delta\varepsilon F\ \mathrm{sinc}^2(F) - C_2\ \mathrm{sinc}(2F)] \tag{10}$$

where $\mathrm{sinc}(x) = \sin(\pi x)/(\pi x)$ is the normalized sinc function, $\Delta\varepsilon$ is the dielectric constant contrast in the grating layer, and C_1 and C_2 are dimensionless constants associated with the strength of the first- and second-order diffraction processes, respectively. See section S1 for details of its derivation. Related to the relative strength of the first order is the bandgap center frequency v, which is the group speed of the guided mode. Note that the first and second terms within the square brackets [...] of Eq. 10 represent the relative strengths of the two sequential first-order diffractions and the single second-order diffraction of the guided mode, respectively. Therefore, a certain desired $m(x)$ distribution due to Eq. 9 can be efficiently translated into a corresponding $F(x)$ distribution.

For example, a flat-top beam is generated by simply having a zero Dirac mass region extended over the desired width around the junction, as shown in Fig. 4. In this calculation, we have considered cylindrical light sources evenly located inside the junction in the same manner as Fig. 2. We assume the emitted beam intensity profile $f(x)$ to be constant over the 6-μm region about the center. The corresponding Dirac mass distribution due to Eq. 9 takes two consecutive steps of three plateaus at m' = −0.634, 0, and +0.635 μm^{-1}, as

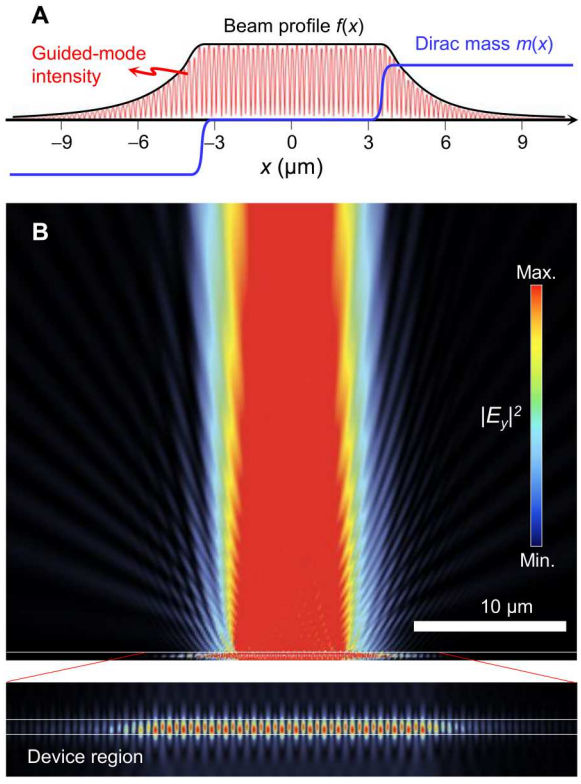

Fig. 4. Flat-top beam generation by Dirac mass control. (**A**) Dirac mass $m(x)$ distribution for flat-top beam generation. It has three plateaus at $m' = -0.634$, 0, and $+0.635\ \mu m^{-1}$, and associated JR state intensity profiles and emitted beam profiles are plotted together for references. (**B**) Electric field intensity $|E_y|^2$ pattern from the structure design based on the Dirac mass distribution in (A). The device structure in this simulation has three grating regions of different fill factors at $F = 0.264$, 0.46, and 0.7, corresponding to the three Dirac mass plateaus. Other device parameters are identical to those for Fig. 1.

indicated in Fig. 4A. This Dirac mass distribution is constructed with experimentally favorable fill factor steps at $F = 0.264$, 0.46, and 0.7 in a GMR structure and generates the desired flat-top beam as shown in Fig. 4B. Therefore, the GMR Dirac mass control can be used for an efficient beam shaping method that is directly applicable to a light emitter.

DISCUSSION

In conclusion, we have proposed a topological junction metasurface for efficient beam emitters with a fundamental advantage of having small angular divergence from the strongly confined radiation area. Characteristic field distributions of a leaky JR state at the junction lead to efficient beaming of light from internal emitters with the help of the cavity-QED coupling and subsequent electromagnetic funneling effects. This topological beaming effect allows direct beam shaping on the resonance state itself for any desired positive definite profile by means of Dirac mass control, which is readily obtainable with moderate fill factor variations in compatible manners with integrated optic architectures on a chip. Therefore, the proposed structure has great potential for creating efficient micro–light emitters taking advantage of strong localization, narrow emission angle, high quantum efficiency, and adaptable beam shaping capability as well. These properties are highly desirable for numerous applications including display pixels (*31*–*34*), solid-state light detection and ranging (*35*, *36*), laser machining (*37*), optical interconnects, and telecommunications (*38*, *39*). Within this context, application to surface-emitting lasers is of immediate interest, although further elaborate studies are required. Introducing the proposed beaming metasurface in semiconductor junction structures may enable highly compact second-order distributed feedback lasers with beam profile adaptation capability. In addition, the topological junction metasurface itself is possibly used as a feedback mechanism in a vertical-cavity surface-emitting laser in the same manner as high-contrast grating reflectors (*40*, *41*), taking advantage of structural simplicity and small footprint size. Moreover, a topological junction mirror can provide additional benefits such as narrow spectral filtering for stable single longitudinal mode operation, feedback efficiency optimization by means of cross-sectional mode matching between the cavity mode and JR state, and emitted beam shaping (*42*).

In another perspective, the proposed method is also directly applicable for efficient optical detectors or absorption-based nanophotonic elements because, in principle, they correspond to the time-reversed emitters (*43*, *44*) that take all such advantages with identical constructions. In this respect, further studies to produce a two-dimensional topological beaming effect are important for the sake of practicality of the proposed concept. We consider that it should be made possible with two-dimensional Dirac mass distributions or bi-grating designs that accommodate higher-order topological states (*45*–*48*). From a broader perspective, our result and an associated follow-up study may motivate various research topics for the development of non-Hermitian topological nanophotonic elements in which interplay between topological states, internal gain or loss, and the external radiation continuum might create novel optical effects and concomitant device applications beyond the present limitations.

MATERIALS AND METHODS

All numerical simulation results here were obtained using a commercial FEM solver (COMSOL Multiphysics). The reflection spectra in Fig. 1B were calculated from the S parameter for an input port emitting a TE-polarized plane wave to the grating structure. The leaky JR eigenstate in Fig. 1C was obtained using the time stationary eigenfrequency solver for a single supercell with the perfectly matched layer (PML) boundary condition. The point emitters generating cylindrical waves were assumed for creating the beaming effects in Figs. 2 to 4. The light sources were evenly distributed inside the junction structure with the PML boundary condition, and we assumed that they generate coherent cylindrical waves at an operation wavelength of 633 nm. For further details of the supercell geometry, light sources, funneling and Purcell effect analyses, and schematic illustrations, see section S2.

Supplementary Materials

This PDF file includes:

Supplementary Text
Figs. S1 to S7

REFERENCES AND NOTES

1. M. Z. Hasan, C. L. Kane, Colloquium: Topological insulators. *Rev. Mod. Phys.* **82**, 3045–3067 (2010).

2. L. Lu, J. D. Joannopoulos, M. Soljačić, Topological photonics. *Nat. Photonics* **8**, 821–829 (2014).
3. T. Ozawa, H. M. Price, A. Amo, N. Goldman, M. Hafezi, L. Lu, M. C. Rechtsman, D. Schuster, J. Simon, O. Zilberberg, I. Carusotto, Topological photonics. *Rev. Mod. Phys.* **91**, 15006 (2019).
4. Y. Lumer, Y. Plotnik, M. C. Rechtsman, M. Segev, Self-localized states in photonic topological insulators. *Phys. Rev. Lett.* **111**, 243905 (2013).
5. M. Hafezi, E. A. Demler, M. D. Lukin, J. M. Taylor, Robust optical delay lines with topological protection. *Nat. Phys.* **7**, 907–912 (2011).
6. J. Noh, W. A. Benalcazar, S. Huang, M. J. Collins, K. P. Chen, T. L. Hughes, M. C. Rechtsman, Topological protection of photonic mid-gap defect modes. *Nat. Photonics* **12**, 408–415 (2018).
7. S. Klembt, T. H. Harder, O. A. Egorov, K. Winkler, R. Ge, M. A. Bandres, M. Emmerling, L. Worschech, T. C. H. Liew, M. Segev, C. Schneider, S. Höfling, Exciton-polariton topological insulator. *Nature* **562**, 552–556 (2018).
8. M. A. Bandres, S. Wittek, G. Harari, M. Parto, J. Ren, M. Segev, D. N. Christodoulides, M. Khajavikhan, Topological insulator laser: Experiments. *Science* **359**, 4003–4005 (2018).
9. M. C. Rechtsman, J. M. Zeuner, Y. Plotnik, Y. Lumer, D. Podolsky, F. Dreisow, S. Nolte, M. Segev, A. Szameit, Photonic Floquet topological insulators. *Nature* **496**, 196–200 (2013).
10. O. Zilberberg, S. Huang, J. Guglielmon, M. Wang, K. P. Chen, Y. E. Kraus, M. C. Rechtsman, Photonic topological boundary pumping as a probe of 4D quantum Hall physics. *Nature* **553**, 59–62 (2018).
11. M. Xiao, Z. . Q. Zhang, C. . T. Chan, Surface impedance and bulk band geometric phases in one-dimensional systems. *Phys. Rev. X* **4**, 021017 (2014).
12. L. H. Wu, X. Hu, Scheme for achieving a topological photonic crystal by using dielectric material. *Phys. Rev. Lett.* **114**, 223901 (2015).
13. S. Barik, A. Karasahin, C. Flower, T. Cai, H. Miyake, W. DeGottardi, M. Hafezi, E. Waks, A topological quantum optics interface. *Science* **359**, 666–668 (2018).
14. B. Zhen, C. W. Hsu, Y. Igarashi, L. Lu, I. Kaminer, A. Pick, S. L. Chua, J. D. Joannopoulos, M. Soljačić, Spawning rings of exceptional points out of Dirac cones. *Nature* **525**, 354–358 (2015).
15. A. Cerjan, S. Huang, M. Wang, K. P. Chen, Y. Chong, M. C. Rechtsman, Experimental realization of a Weyl exceptional ring. *Nat. Photonics* **13**, 623–628 (2019).
16. H. Zhou, C. Peng, Y. Yoon, C. W. Hsu, K. A. Nelson, L. Fu, J. D. Joannopoulos, M. Soljačić, B. Zhen, Observation of bulk Fermi arc and polarization half charge from paired exceptional points. *Science* **359**, 1009–1012 (2018).
17. K. Y. Lee, K. W. Yoo, S. Cheon, W.-J. Joo, J. W. Yoon, S. H. Song, Synthetic topological nodal phase in bilayer resonant gratings. *Phys. Rev. Lett.* **128**, 53002 (2022).
18. B. Wang, W. Liu, M. Zhao, J. Wang, Y. Zhang, A. Chen, F. Guan, X. Liu, L. Shi, J. Zi, Generating optical vortex beams by momentum-space polarization vortices centred at bound states in the continuum. *Nat. Photonics* **14**, 623–628 (2020).
19. Q. Song, M. Odeh, J. Zúñiga-Pérez, B. Kanté, P. Genevet, Plasmonic topological metasurface by encircling an exceptional point. *Science* **373**, 1133–1137 (2021).
20. K. Y. Lee, K. W. Yoo, Y. Choi, G. Kim, S. Cheon, J. W. Yoon, S. H. Song, Topological guided-mode resonances at non-Hermitian nanophotonic interfaces. *Nanophotonics* **10**, 1853–1860 (2021).
21. Y. C. Jun, K. C. Y. Huang, M. L. Brongersma, Plasmonic beaming and active control over fluorescent emission. *Nat. Commun.* **2**, 283 (2011).
22. H. J. Lezec, A. Degiron, E. Devaux, R. A. Linke, L. Martin-Moreno, F. J. Garcia-Vidal, T. W. Ebbesen, Beaming light from a subwavelength aperture. *Science* **297**, 820–822 (2002).
23. L. Martín-Moreno, F. J. García-Vidal, H. J. Lezec, A. Degiron, T. W. Ebbesen, Theory of highly directional emission from a single subwavelength aperture surrounded by surface corrugations. *Phys. Rev. Lett.* **90**, 167401 (2003).
24. P. Kramper, M. Agio, C. M. Soukoulis, A. Birner, F. Müller, R. B. Wehrspohn, U. Gösele, V. Sandoghdar, Highly directional emission from photonic crystal waveguides of subwavelength width. *Phys. Rev. Lett.* **92**, 113903 (2004).
25. E. Moreno, F. J. García-Vidal, L. Martín-Moreno, Enhanced transmission and beaming of light via photonic crystal surface modes. *Phys. Rev. B* **69**, 121402 (2004).
26. A. Vaskin, R. Kolkowski, A. F. Koenderink, I. Staude, Light-emitting metasurfaces. *Nanophotonics* **8**, 1151–1198 (2019).
27. F. Pardo, P. Bouchon, R. Haïdar, J.-L. Pelouard, Light funneling mechanism explained by magnetoelectric interference. *Phys. Rev. Lett.* **107**, 093902 (2011).
28. P. Zhu, P. Jin, H. Shi, L. J. Guo, Funneling light into subwavelength grooves in metal/dielectric multilayer films. *Opt. Express* **21**, 3595–3602 (2013).
29. J. W. Li, J. S. Hong, W. T. Chou, D. J. Huang, K. R. Chen, Light funneling profile during enhanced transmission through a subwavelength metallic slit. *Plasmonics* **13**, 2249–2254 (2018).
30. Z. Qian, Z. Li, H. Hao, L. Shan, Q. Zhang, J. Dong, Q. Gong, Y. Gu, Absorption reduction of large purcell enhancement enabled by topological state-led mode coupling. *Phys. Rev. Lett.* **126**, 023901 (2021).
31. W.-J. Joo, J. Kyoung, M. Esfandyarpour, S.-H. Lee, H. Koo, S. Song, Y.-N. Kwon, S. H. Song, J. C. Bae, A. Jo, M.-J. Kwon, S. H. Han, S.-H. Kim, S. Hwang, M. L. Brongersma, Metasurface-driven OLED displays beyond 10,000 pixels per inch. *Science* **370**, 459–463 (2020).
32. K. Kumar, H. Duan, R. S. Hegde, S. C. W. Koh, J. N. Wei, J. K. W. Yang, Printing colour at the optical diffraction limit. *Nat. Nanotechnol.* **7**, 557–561 (2012).
33. Y. Mohtashami, R. A. De Crescent, L. K. Heki, P. P. Iyer, N. A. Butakov, M. S. Wong, A. Alhassan, W. J. Mitchell, S. Nakamura, S. P. Den Baars, J. A. Schuller, Light-emitting metalenses and meta-axicons for focusing and beaming of spontaneous emission. *Nat. Commun.* **12**, 3591 (2021).
34. J.-H. Song, J. van de Groep, S. J. Kim, M. L. Brongersma, Non-local metasurfaces for spectrally decoupled wavefront manipulation and eye tracking. *Nat. Nanotechnol.* **16**, 1224–1230 (2021).
35. I. Kim, R. J. Martins, J. Jang, T. Badloe, S. Khadir, H.-Y. Jung, H. Kim, J. Kim, P. Genevet, J. Rho, Nanophotonics for light detection and ranging technology. *Nat. Nanotechnol.* **16**, 508–524 (2021).
36. J. Park, B. G. Jeong, S. I. Kim, D. Lee, J. Kim, C. Shin, C. B. Lee, T. Otsuka, J. Kyoung, S. Kim, K.-Y. Yang, Y.-Y. Park, J. Lee, I. Hwang, J. Jang, S. H. Song, M. L. Brongersma, K. Ha, S.-W. Hwang, H. Choo, B. L. Choi, All-solid-state spatial light modulator with independent phase and amplitude control for three-dimensional LiDAR applications. *Nat. Nanotechnol.* **16**, 69–76 (2021).
37. P. S. Salter, M. J. Booth, Adaptive optics in laser processing. *Light Sci. Appl.* **8**, 110 (2019).
38. Y.-Y. Xie, P.-N. Ni, Q.-H. Wang, Q. Kan, G. Briere, P.-P. Chen, Z.-Z. Zhao, A. Delga, H.-R. Ren, H.-D. Chen, C. Xu, P. Genevet, Metasurface-integrated vertical cavity surface-emitting lasers for programmable directional lasing emissions. *Nat. Nanotechnol.* **15**, 125–130 (2020).
39. P. Moser, J. A. Lott, D. Bimberg, Energy efficiency of directly modulated oxide-confined high bit rate 850-nm VCSELs for optical interconnects. *IEEE J. Sel. Top. Quantum Electron.* **19**, 1702212 (2014).
40. Y. Zhou, M. Moewe, J. Kern, M. C. Huang, C. J. Chang-Hasnain, Surface-normal emission of a high-Q resonator using a subwavelength high-contrast grating. *Opt. Express* **16**, 17282–17287 (2008).
41. Y. Zhou, M. C. Y. Huang, C. Chase, V. Karagodsky, M. Moewe, B. Pesala, F. G. Sedgwick, C. Chang-Hasnain, High-index-contrast grating (HCG) and its applications in optoelectronic devices. *IEEE J. Sel. Top. Quantum Electron.* **15**, 1485–1499 (2009).
42. R. Contractor, W. Noh, W. Redjem, W. Qarony, E. Martin, S. Dhuey, A. Schwartzberg, B. Kanté, Scalable single-mode surface-emitting laser via open-Dirac singularities. *Nature* **608**, 692–698 (2022).
43. W. Wan, Y. Chong, L. Ge, H. Noh, A. D. Stone, H. Cao, Time-reversed lasing and interferometric control of absorption. *Science* **331**, 889–892 (2011).
44. J. W. Yoon, G. M. Koh, S. H. Song, R. Magnusson, Measurement and modeling of a complete optical absorption and scattering by coherent surface plasmon-polariton excitation using a silver thin-film grating. *Phys. Rev. Lett.* **109**, 257402 (2012).
45. W. A. Benalcazar, B. A. Bernevig, T. L. Hughes, Quantized electric multipole insulators. *Science* **357**, 61–66 (2017).
46. B. Xie, H.-X. Wang, X. Zhang, P. Zhan, J.-H. Jiang, M. Lu, Y. Chen, Higher-order band topology. *Nat. Rev. Phys.* **3**, 520–532 (2021).
47. M. Kim, Z. Jacob, J. Rho, Recent advances in 2D, 3D and higher-order topological photonics. *Light Sci. Appl.* **9**, 130 (2020).
48. H.-R. Kim, M.-S. Hwang, D. Smirnova, K.-Y. Jeong, Y. Kivshar, H.-G. Park, Multipolar lasing modes from topological corner states. *Nat. Commun.* **11**, 5758 (2020).

Acknowledgments

Funding: This research was supported in part by the Leader Researcher Program (NRF-2019R1A3B2068083), the Basic Science Research Program (NRF-2018R1A2B3002539), and the research fund of Hanyang University (HY-202000000000513). K.Y.L. acknowledges the NRF Sejong Science fellowship (NRF-2022R1C1C2006290) funded by the MSIT of the Korean government. **Author contributions:** Conceptualization: K.Y.L., J.W.Y., and S.H.S. Methodology: K.Y.L., S.Y., and J.W.Y. Investigation: K.Y.L., J.W.Y., and S.H.S. Visualization: K.Y.L. Supervision: J.W.Y. Writing—original draft: K.Y.L. and J.W.Y. Writing—review and editing: K.Y.L., J.W.Y., and S.H.S. **Competing interests:** The authors declare that they have no competing interests. **Data and materials availability:** All data needed to evaluate the conclusions in the paper are present in the paper and/or the Supplementary Materials.

Submitted 7 July 2022
Accepted 1 November 2022
Published 9 December 2022
10.1126/sciadv.add8349

ScienceAdvances

Topological beaming of light

Ki Young Lee, Seungjin Yoon, Seok Ho Song, and Jae Woong Yoon

Sci. Adv., **8** (49), eadd8349.
DOI: 10.1126/sciadv.add8349

Science Advances (ISSN) is published by the American Association for the Advancement of Science. 1200 New York Avenue NW, Washington, DC 20005. The title *Science Advances* is a registered trademark of AAAS.